Available online at www.sciencedirect.com

ScienceDirect

Nuclear Physics B 916 (2017) 669–687

NUCLEAR PHYSICS B

www.elsevier.com/locate/nuclphysb

Stable strange quark matter objects with running masses and coupling constant

Cheng-Jun Xia [a,b,*], Shan-Gui Zhou [b,c,d,e]

[a] *School of Information Science and Engineering, Ningbo Institute of Technology, Zhejiang University, Ningbo 315100, China*

[b] *CAS Key Laboratory of Theoretical Physics, Institute of Theoretical Physics, Chinese Academy of Sciences, Beijing 100190, China*

[c] *School of Physics, University of Chinese Academy of Sciences, Beijing 100049, China*

[d] *Center of Theoretical Nuclear Physics, National Laboratory of Heavy Ion Accelerator, Lanzhou 730000, China*

[e] *Synergetic Innovation Center for Quantum Effects and Application, Hunan Normal University, Changsha 410081, China*

Received 22 December 2016; received in revised form 18 January 2017; accepted 21 January 2017

Available online 27 January 2017

Editor: Hong-Jian He

Abstract

We improve our recently proposed unified description for strange quark matter (SQM) objects, in the way that analytical expressions are derived and used to calculate the distribution of particles inside an SQM object. In the improved model, the computational time is greatly reduced without losing accuracy. The properties of SQM objects are then investigated by adopting perturbative quantum chromodynamics (pQCD) with running quark masses and coupling constant. Aside from the increase of masses and radii of strange stars, it is found that the perturbative interactions also make the electric field on the surface stronger and extends deeper into the core, while small SQM objects become less compact and more positively charged. These may affect the experimental searches of SQM.

* Corresponding author.
E-mail address: cjxia@itp.ac.cn (C.-J. Xia).

http://dx.doi.org/10.1016/j.nuclphysb.2017.01.022

1. Introduction

Due to the asymptotic freedom of strong interactions, strange quark matter (SQM) is formed at high enough densities. Unlike ordinary nuclear matter, SQM consists of approximately equal numbers of up, down, and strange quarks. Early studies of SQM with effective models suggested its absolute stability [1–3], indicating the possible existence of stable SQM objects such as strangelets [4–7], nuclearites [8,9], meteorlike compact ultradense objects [10], and strange stars [11–19].

The properties of these SQM objects have been studied extensively. For example, with nonzero strange quark masses, it was found that strangelets in perfect weak equilibrium are slightly positively charged [4]. Strong parameter dependence was revealed for their properties [20,21]. The possible formation of strangelets in heavy-ion collisions was investigated [22,23], and it was proposed that strangelets which are stable against strong decay are most likely highly negatively charged [24]. By constraining its shape in an axially symmetric bag, it was found that a strangelet is in favor of spherical shape [25]. Since the wave functions of quarks approach to zero on the quark-vacuum interface, there are surface effects caused by quark depletion, which can be well described with the multiple reflection expansion (MRE) method [5,26–28]. Adopting a small enough surface tension, a strangelet at certain size is more stable than others if the effects of charge screening are considered [29]. In such cases, the surface of a strange star may consist of a crystalline crust comprised of SQM nuggets embedded in a uniform electron background [30]. Considering the electron–positron pair creation in the supercritical electric field of a static spherical object, an upper bound on the net charge of SQM objects was obtained [31]. The properties of strangelets and strange stars were thoroughly investigated using the equivparticle model [32–39].

If SQM objects are absolutely stable, there may be a chance for us to observe them. Up till now, several incidents that fit the SQM characteristics have been detected [40–43], while more efforts are being made for the search of SQM [44–46]. On the other hand, since its first discovery [47], approximately 2,500 pulsars have been found [48]. The extreme conditions of pulsars offer us a unique opportunity to study matter at highest densities, where SQM may be favored. In fact, there are several hints suggesting that pulsars may actually be strange stars [49–51]. Nevertheless, final confirmation may rely on future observations, e.g., the lightweight asymmetry and magnetism probe (LAMP) project [52], the five-hundred-meter aperture spherical telescope (FAST) [53], the neutron star interior composition explorer (NICER) [54], and the square kilometre array (SKA) [55], etc.

Recently, we have proposed a unified description for SQM objects [56–58], called hereafter the UDS model. The properties of these objects ranging from strangelets to strange stars were investigated, where the MIT bag model was adopted for the local properties of SQM. The numerical calculation was carried out in a straightforward manner, and was time consuming. In this paper, with certain approximations, we obtain the analytical expressions for the distribution functions of particles, which significantly reduces the computational time. The interaction between quarks was ignored in our previous work. However, recent studies via relativistic heavy ion collisions indicate that quarks are strongly correlated [59]. In fact, according to the precise mass measurements of PSR J1614-2230 ($1.928 \pm 0.017\ M_\odot$) [60,61] and PSR J0348+0432 ($2.01 \pm 0.04\ M_\odot$) [62], it is unlikely that the masses of strange stars predicted with bag model can reach these observational values, while including the perturbative interactions can change this situation [63–65]. Knowing that the interaction between quarks is negligible only at much lager densities, it is thus necessary to include the perturbative interactions in our calculation.

In this work, we investigate the properties of SQM objects by adopting perturbative quantum chromodynamics (pQCD), while the renormalization scale and the energy difference between the physical and perturbative vacua are treated with phenomenological approaches.

The paper is organized as follows. In Sec. 2.1 we present the formalism of pQCD with necessary non-perturbative corrections. For the particle distributions of an SQM object, we adopt the UDS model in Sec. 2.2 with certain approximations to simplify our calculation. The average effects of quark depletion on the quark-vacuum interface are treated with the MRE method in Sec. 2.3. Our results are presented in Sec. 3, where the properties of β-stable SQM with local charge neutrality and SQM objects are investigated in Secs. 3.1 and 3.2. We draw our conclusion in Sec. 4.

2. Theoretical framework

2.1. SQM with pQCD

The pQCD thermodynamic potential of cold quark matter consisting of massless quarks was obtained by Freedman and McLerran in 1977 [66]. Later on, it was realized that the contribution of the nonvanishing strange quark mass is sizable [63]. Thus, here we adopt pQCD with the quark masses and strong coupling constant running with the energy scale. Currently, the state-of-the-art pQCD calculations were performed to the order of α_s^2 [64], where α_s is the renormalized strong coupling constant of QCD Lagrangian. In this work, we adopt these results up to the order of α_s, where the thermodynamic potential density in the $\overline{\text{MS}}$ scheme is given by [63]

$$\Omega^{\text{pt}} = \sum_i^{N_f} \left(\omega_i^0 + \omega_i^1 \alpha_s\right), \tag{1}$$

with

$$\omega_i^0 = -\frac{g_i m_i^4}{24\pi^2}\left[u_i v_i \left(u_i^2 - \frac{5}{2}\right) + \frac{3}{2}\ln(u_i + v_i)\right], \tag{2}$$

$$\omega_i^1 = \frac{g_i m_i^4}{12\pi^3}\left\{\left[6\ln\left(\frac{\bar{\Lambda}}{m_i}\right) + 4\right][u_i v_i - \ln(u_i + v_i)] + 3\,[u_i v_i - \ln(u_i + v_i)]^2 - 2v_i^4\right\}. \tag{3}$$

Here $u_i \equiv \mu_i/m_i$ and $v_i \equiv \sqrt{u_i^2 - 1}$ with μ_i, m_i, and g_i ($g_u = g_d = g_s = 6$, $g_e = 2$) being the chemical potential, mass, and degeneracy factor for particle type i, respectively.

The running coupling constant and masses are obtained with the β-function and γ-function, i.e.,

$$\frac{\mathrm{d}\alpha_s}{\mathrm{d}\bar{\Lambda}} = -\frac{2}{\bar{\Lambda}}\sum_{i=0}^{\infty}\beta_i \alpha_s^{i+2}, \tag{4}$$

$$\frac{\mathrm{d}m_i}{\mathrm{d}\bar{\Lambda}} = -\frac{2m_i}{\bar{\Lambda}}\sum_{i=0}^{\infty}\gamma_i \alpha_s^{i+1}. \tag{5}$$

Those functions are known up to 4-loop order in the $\overline{\text{MS}}$ scheme [67,68]. Ignore the higher order terms, we take $\beta_0 = \frac{1}{4\pi}(11 - \frac{2}{3}N_f)$ and $\beta_1 = \frac{1}{16\pi^2}(102 - \frac{38}{3}N_f)$ for the β-function while

$\gamma_0 = 1/\pi$ and $\gamma_1 = \frac{1}{16\pi^2}(\frac{202}{3} - \frac{20}{9}N_{\rm f})$ for the γ-function. Then the scale dependence of the strong coupling constant and mass are given by

$$\alpha_{\rm s}(\bar{\Lambda}) = \frac{1}{\beta_0 L}\left(1 - \frac{\beta_1 \ln L}{\beta_0^2 L}\right), \tag{6}$$

$$m_i(\bar{\Lambda}) = \hat{m}_i \alpha_{\rm s}^{\frac{\gamma_0}{\beta_0}}\left[1 + \left(\frac{\gamma_1}{\beta_0} - \frac{\beta_1\gamma_0}{\beta_0^2}\right)\alpha_{\rm s}\right], \tag{7}$$

where $L = 2\ln\left(\frac{\bar{\Lambda}}{\Lambda_{\overline{\rm MS}}}\right)$ with $\Lambda_{\overline{\rm MS}}$ being the $\overline{\rm MS}$ renormalization point. At present, it is not clear how exactly the renormalization scale $\bar{\Lambda}$ evolves with the chemical potentials of quarks. There are various choices, e.g., $\bar{\Lambda} = C\sum_i \mu_i/N_{\rm f}$ [63], $\bar{\Lambda} = C\sqrt[4]{\sum_i \mu_i^4/N_{\rm f}}$ [19], etc. In this work, we expand $\bar{\Lambda}$ with respect to the average value of quark chemical potentials and take to the first-order

$$\bar{\Lambda} = C_0 + \frac{C_1}{N_{\rm f}}\sum_i \mu_i, \tag{8}$$

where $C_0 = 0 \sim 1$ GeV and $C_1 = 1 \sim 4$ [65].

To incorporate the non-perturbative corrections, we introduce an extra bag constant B to take into account the energy difference between the physical and perturbative vacua. The modified thermodynamic potential density for SQM is

$$\Omega = \Omega^{\rm pt} + \omega_e^0 + B. \tag{9}$$

Here the contribution of electrons is indicated as ω_e^0, which is obtained with Eq. (2).

Based on the basic thermodynamic relations, the particle number density is given by

$$n_i = -\left.\frac{\partial\Omega}{\partial\mu_i}\right|_{\mu_{j\neq i}}. \tag{10}$$

For quarks, the particle number density obtained with Eq. (10) can be divided into two parts, i.e.,

$$n_i = n_i^* + n_0, \tag{11}$$

with

$$n_i^* = -\left.\frac{\partial\omega_i^0}{\partial\mu_i}\right|_{m_i} - \left.\frac{\partial\omega_i^1}{\partial\mu_i}\right|_{m_i,\bar{\Lambda}}\alpha_{\rm s}, \tag{12}$$

$$n_0 = -\sum_k^{N_f}\left(\left.\frac{\partial\omega_k^0}{\partial m_k}\right|_{\mu_k}\frac{{\rm d}m_k}{{\rm d}\bar{\Lambda}} + \left.\frac{\partial\omega_k^1}{\partial m_k}\right|_{\mu_k,\bar{\Lambda}}\frac{{\rm d}m_k}{{\rm d}\bar{\Lambda}}\alpha_{\rm s} + \left.\frac{\partial\omega_k^1}{\partial\bar{\Lambda}}\right|_{\mu_k,m_k}\alpha_{\rm s} + \omega_k^1\frac{{\rm d}\alpha_{\rm s}}{{\rm d}\bar{\Lambda}}\right)\left.\frac{\partial\bar{\Lambda}}{\partial\mu_i}\right|_{\mu_{j\neq i}}. \tag{13}$$

Here n_0 arises due to the scale dependence of the strong coupling constant and quark masses. If we take constant values for $\alpha_{\rm s}$ and m_i, n_0 vanishes. Note that for the derivatives of $\alpha_{\rm s}$ and m_i, instead of adopting the β-function and γ-function in Eqs. (4) and (5), we take the derivatives of Eqs. (6) and (7) and keep the higher order terms to avoid thermodynamic inconsistency, i.e.,

$$\frac{\mathrm{d}\alpha_\mathrm{s}}{\mathrm{d}\bar{\Lambda}} = -2\frac{\beta_0^2 L - 2\beta_1 \ln(L) + \beta_1}{\beta_0^3 L^3 \bar{\Lambda}}, \tag{14}$$

$$\frac{\mathrm{d}m_i}{\mathrm{d}\bar{\Lambda}} = \hat{m}_i \frac{\gamma_0}{\beta_0} \alpha_\mathrm{s}^{\gamma_0/\beta_0} \left[\frac{1}{\alpha_\mathrm{s}} + \left(\frac{\gamma_1}{\gamma_0} - \frac{\beta_1}{\beta_0}\right)\left(1 + \frac{\gamma_0}{\beta_0}\right)\right] \frac{\mathrm{d}\alpha_\mathrm{s}}{\mathrm{d}\bar{\Lambda}}. \tag{15}$$

For electrons, the number density given by Eq. (10) reads

$$n_e = -\left.\frac{\partial \omega_e^0}{\partial \mu_e}\right|_{m_e} = \frac{(\mu_e^2 - m_e^2)^{3/2}}{3\pi^2}. \tag{16}$$

The energy density and pressure of electrons are $E_e = \omega_e^0 + \mu_e n_e$ and $P_e = -\omega_e^0$, respectively.

Then the energy density for SQM is obtained with

$$E = \Omega^\mathrm{pt} + \omega_e^0 + B + \sum_i \mu_i n_i, \tag{17}$$

while the pressure takes negative values of the thermodynamic potential density, i.e., $P = -\Omega$.

Due to the weak reactions such as $d, s \leftrightarrow u + e + \bar{\nu}_e$ and $s + u \leftrightarrow u + d$, quarks can be converted into each other. For stable SQM, the β-equilibrium condition needs to be satisfied, i.e.,

$$\mu_u + \mu_e = \mu_d = \mu_s. \tag{18}$$

Here the chemical potential of neutrinos are set to zero since they can leave the system freely.

2.2. The distribution functions

For zero temperature cases, the internal structure of a static SQM object is determined by minimizing the mass at given number of particles. The local chemical potential $\mu_i(r)$ of a spherically symmetric SQM object at ground state follows [56–58]

$$\bar{\mu}_i = \mu_i(r)\mathrm{e}^{\nu(r)/2} + q_i\varphi(r) = \text{constant}, \tag{19}$$

with the metric elements $\mathrm{e}^{\nu(r)}$ and $\mathrm{e}^{\lambda(r)}$ as well as the electric potential $\varphi(r)$ determined by

$$\nu' = \frac{2G\mathrm{e}^\lambda}{r^2}\left[4\pi r^3\left(P - \frac{\alpha Q^2}{8\pi r^4}\right) + M_\mathrm{t}\right], \tag{20}$$

$$\mathrm{e}^{-\lambda} = 1 - \frac{2G}{r}M_\mathrm{t}, \tag{21}$$

$$\varphi' = -\frac{\alpha Q}{r^2}\mathrm{e}^{(\lambda+\nu)/2}. \tag{22}$$

In this work we use the natural system of units and adopt the "prime notion" so that $\nu' = \mathrm{d}\nu/\mathrm{d}r$ and $\varphi' = \mathrm{d}\varphi/\mathrm{d}r$. The gravitational constant and fine-structure constant are taken as $G = 6.707 \times 10^{-45}$ MeV^{-2} and $\alpha = 1/137$, respectively. The total mass M_t, particle number N_i, and charge Q enclosed in a sphere with radius r are

$$M_\mathrm{t}(r) = \int_0^r 4\pi\bar{r}^2\left(E + \frac{\alpha Q^2}{8\pi\bar{r}^4}\right)\mathrm{d}\bar{r}, \tag{23}$$

$$N_i(r) = \int_0^r 4\pi \bar{r}^2 n_i \mathrm{e}^{\lambda/2} \mathrm{d}\bar{r}, \tag{24}$$

$$Q(r) = \sum_i q_i N_i(r) = \int_0^r 4\pi \bar{r}^2 n_{\mathrm{ch}} \mathrm{e}^{\lambda/2} \mathrm{d}\bar{r}. \tag{25}$$

Here $n_i(r)$ is the local number density of particle type i, which determines the local charge density $n_{\mathrm{ch}}(r) = \sum_i q_i n_i(r)$ with the particle charge $q_u = \frac{2}{3}$, $q_d = q_s = -\frac{1}{3}$, and $q_e = -1$. Meanwhile, the pressure $P(r)$ and energy density $E(r)$ are also related to the local properties of SQM.

Based on Eq. (19) and the Thomas–Fermi approximation, the structure of an SQM object is unambiguously determined by $\varphi(r)$ and $\nu(r)$ at given $\bar{\mu}_i$, which gives the local chemical potential $\mu_i(r) = \left[\bar{\mu}_i - q_i\varphi(r)\right]\mathrm{e}^{-\nu(r)/2}$. The particle distribution of an SQM object can then be obtained by solving the differential equations (20) and (22) along with the subsidiary conditions (21), (23)–(25). It is found that the structure of an SQM object resembles an atom, consisting of a positively charged quark core surrounded by an electron cloud [56–58].

A straightforward calculation of the aforementioned formulae consumes many computational resources. To simplify our calculation, we substitute Eq. (22) into Eq. (25) and take the derivative with respect to r, which gives

$$r^2\varphi'' + 2r\varphi' - \frac{\lambda' + \nu'}{2} r^2\varphi' + 4\pi\alpha r^2 n_{\mathrm{ch}} \mathrm{e}^{\lambda} \mathrm{e}^{\nu/2} = 0. \tag{26}$$

2.2.1. The electric field of the quark part

It is convenient for us to solve the differential equation (26) approximately by expanding the charge density $n_{\mathrm{ch}}(\varphi, \nu)$ and keeping the leading terms:

$$n_{\mathrm{ch}}(\varphi, \nu) \approx \left.\frac{\partial n_{\mathrm{ch}}}{\partial \varphi}\right|_{\nu} \Delta\varphi + \left.\frac{\partial n_{\mathrm{ch}}}{\partial \nu}\right|_{\varphi} \Delta\nu. \tag{27}$$

Here we have defined $\Delta\varphi = \varphi - \varphi_0$ and $\Delta\nu = \nu - \nu_0$ with $n_{\mathrm{ch}}(\varphi_0, \nu_0) = 0$. For the differential equation

$$r^2\varphi_{\mathrm{S}}'' + 2r\varphi_{\mathrm{S}}' + 4\pi\alpha r^2 \mathrm{e}^{\lambda_0} \mathrm{e}^{\nu_0/2} \left.\frac{\partial n_{\mathrm{ch}}}{\partial \varphi}\right|_{\nu} \varphi_{\mathrm{S}} = 0, \tag{28}$$

it can be solved analytically and gives

$$\varphi_{\mathrm{S}}(r) = \frac{c_1}{r} \mathrm{e}^{(r-R)/\bar{\lambda}_{\mathrm{D}}} + \frac{c_2}{r} \mathrm{e}^{-(r-R)/\bar{\lambda}_{\mathrm{D}}}, \tag{29}$$

where

$$\bar{\lambda}_{\mathrm{D}}^{-2} = -4\pi\alpha \mathrm{e}^{\lambda_0} \mathrm{e}^{\nu_0/2} \left.\frac{\partial n_{\mathrm{ch}}}{\partial \varphi}\right|_{\nu} = \mathrm{e}^{\lambda_0} \lambda_{\mathrm{D}}^{-2}. \tag{30}$$

Here R represents the radius of the quark core and $\lambda_{\mathrm{D}} \equiv \left(4\pi\alpha \sum_i q_i \left.\frac{\partial n_{\mathrm{ch}}}{\partial \mu_i}\right|_{\mu_j \neq i}\right)^{-1/2}$ is the Debye screening length of SQM [69].

Now the electric field can be divided into three parts, i.e.,

$$\varphi(r) = \varphi_{\mathrm{S}}(r) + \varphi_{\mathrm{G}}(r) + \varphi_0, \tag{31}$$

where $\varphi_{\rm G}(r)$ takes account of the gravitational effect on the electric field and is comparatively small. By substituting Eq. (31) into Eq. (26) with the charge density given by Eq. (27), we obtain

$$\varphi_{\rm G}(r) = -\Delta\nu \left.\frac{\partial n_{\rm ch}}{\partial \nu}\right|_{\varphi} \Big/ \left.\frac{\partial n_{\rm ch}}{\partial \varphi}\right|_{\nu} - \frac{\lambda' + \nu'}{2}\bar{\lambda}_{\rm D}^2\varphi_{\rm S}'. \tag{32}$$

The derivative terms of $\varphi_{\rm G}$ are neglected since their contributions are insignificant. Meanwhile, the last term in Eq. (32) is small enough to be ignored even when $\varphi_{\rm S}$ is sizable. To obtain $\varphi_{\rm G}(r)$ throughout the quark part, we take the derivative of Eq. (32) with respect to r and discard higher order contributions, i.e.,

$$\varphi_{\rm G}'(r) = 4\pi\alpha {\rm e}^{\nu(r)/2}\lambda_{\rm D}(r)^2 \left.\frac{\partial n_{\rm ch}}{\partial \nu}\right|_{\varphi} \nu'(r). \tag{33}$$

Then $\varphi_{\rm G}(r)$ is obtained by integrating Eq. (33).

At the center of an SQM object ($r = 0$), according to Eq. (22) and Eq. (33), we have $r^2\varphi'(r) = r^2\left[\varphi_{\rm S}'(r) + \varphi_{\rm G}'(r)\right] = 0$ and $\varphi_{\rm G}'(r) = 0$ since $Q(0) = 0$ and $\nu'(0) = 0$. Then Eq. (29) satisfies $\lim_{r\to 0} r^2\varphi_{\rm S}'(r) = 0$, which gives

$$\varphi_{\rm S} = \frac{c_1}{r}\left[{\rm e}^{(r-R)/\bar{\lambda}_{\rm D}} - {\rm e}^{-(r+R)/\bar{\lambda}_{\rm D}}\right]. \tag{34}$$

Finally, the electric field within the quark core is obtained with Eq. (31), where $\varphi_{\rm G}$ and $\varphi_{\rm S}$ are determined by Eqs. (33) and (34), respectively. Note that at $r = R$, we take $\varphi_{\rm G}(R) = 0$ and $\nu(R) = \nu_0$.

2.2.2. The electric field of the electron cloud

According to Eq. (26), the electric field of the electron cloud ($r > R$) can be obtained with

$$r^2\varphi'' + 2r\varphi' - \frac{\lambda' + \nu'}{2}r^2\varphi' - 4\pi\alpha r^2 n_e {\rm e}^{\lambda}{\rm e}^{\nu/2} = 0. \tag{35}$$

Generally speaking, the electron cloud covers an extremely thin layer ($\sim$1 Å) in the surface region with little contribution to the total mass so that the metric elements remain constant, i.e., ${\rm e}^{\lambda(r)} \approx {\rm e}^{-\nu(r)} \approx {\rm e}^{\lambda(R)} =$ constant at $r \approx R$. Then Eq. (35) becomes

$$\bar{\varphi}'' + 2\bar{\varphi}'/r - 4\pi\alpha n_e {\rm e}^{\lambda} = 0, \tag{36}$$

with $\bar{\varphi} \equiv \varphi {\rm e}^{-\nu/2}$ and the electron number density determined by Eq. (16). Since the global charge neutrality condition is fulfilled, we have $\bar{\mu}_e {\rm e}^{-\nu(R)/2} = m_e$. The local electron chemical potential is then obtained with $\mu_e(r) = \bar{\varphi}(r) + m_e$.

If the core radius R is large enough, the second term in Eq. (36) can be ignored [70]. Assuming zero electron mass $m_e = 0$ and take $\bar{\mu}_e = 0$, the local chemical potential of electrons becomes $\mu_e(r) = \bar{\varphi}(r)$. Then the electron number density is obtained with

$$n_e = \frac{\mu_e^3}{3\pi^2} = \frac{\bar{\varphi}^3}{3\pi^2}, \tag{37}$$

and Eq. (36) becomes

$$\bar{\varphi}'' - \frac{4\alpha}{3\pi} e^{\lambda} \bar{\varphi}^3 = 0. \tag{38}$$

This equation can be solved analytically at given $\bar{\varphi}(R)$ by satisfying the boundary condition $\bar{\varphi}(\infty) = 0$, which gives

$$\bar{\varphi}(r) = \frac{\bar{\varphi}(R)}{\kappa(r-R)+1}, \tag{39}$$

with $\kappa \equiv \sqrt{\frac{2\alpha}{3\pi}} \bar{\varphi}(R) e^{\lambda(R)/2}$.

For massless electrons, the particle number density is determined by Eq. (37), while the energy density is $E_e = \mu_e^4/4\pi^2$ and pressure $P_e = \mu_e^4/12\pi^2$. According to Eqs. (22) and (23), the mass contribution from the electron cloud reads

$$M_e = \int_R^\infty r^2 \left(\frac{\bar{\varphi}^4}{\pi} + \frac{\varphi'^2}{2\alpha} \right) dr = \frac{\bar{\varphi}(R)^2}{6\pi\alpha\kappa^3} \left(R^2\kappa^2 + R\kappa + 1 \right) \left[e^{-\lambda(R)} \pi\kappa^2 + 2\alpha\bar{\varphi}(R)^2 \right]. \tag{40}$$

2.3. The surface

Since the wave functions approach to zero on the surface of an SQM object, quarks are depleted and consequently contribute to the interface effects. By counting the number of depleted quarks, the average effects due to quark depletion are treated with a modification to the density of states. Here we adopt the multiple reflection expansion (MRE) method [5,26–28], which gives

$$n_i^{\rm surf}(p_i) = -\frac{g_i R^2 p_i}{\pi} \arctan\left(\frac{m_i}{p_i}\right) + \frac{2 g_i R}{3\pi} \left[1 - \frac{3 p_i}{2 m_i} \arctan\left(\frac{m_i}{p_i}\right) \right], \tag{41}$$

with p_i being the momentum of quark flavor i ($i = u, d, s$). The upper bound of p_i corresponds to the Fermi momentum on the interface $\nu_i(R)$ and is obtained phenomenologically by solving $g_i \nu_i(R)^3/6\pi^2 = n_i$ with n_i given by Eq. (10). Then the corresponding contributions to particle number $N_i^{\rm surf}$, energy $\bar{E}_i^{\rm surf}$, and pressure $P^{\rm surf}$ are determined by

$$N_i^{\rm surf} = \int_0^{\nu_i(R)} n_i^{\rm surf}(p_i) dp_i, \tag{42}$$

$$\bar{E}_i^{\rm surf} = \int_0^{\nu_i(R)} \sqrt{p_i^2 + m_i^2}\, n_i^{\rm surf}(p_i) dp_i, \tag{43}$$

$$P^{\rm surf} = -\sum_i \left. \frac{d\bar{E}_i^{\rm surf}}{dV} \right|_{N_i^{\rm surf}}. \tag{44}$$

The surface charge created by quark depletion is obtained with $Q^{\rm surf} = \sum_i q_i N_i^{\rm surf}$. Due to the presence of gravity, the contribution to the mass of an SQM object is

$$M^{\rm surf} = \sum_i \bar{E}_i^{\rm surf} {\rm e}^{\nu(R)/2}, \tag{45}$$

with $\bar{E}_i^{\rm surf}$ given by Eq. (43).

On the requirement of dynamic stability of the quark-vacuum interface, the outward pressure of quarks should match the inward vacuum pressure B, i.e.,

$$P(R) - P_e(R) + P^{\rm surf} = 0. \tag{46}$$

Finally, by satisfying the continuity condition at $r = R$

$$\varphi(R^-) = \varphi(R^+), \tag{47}$$

$$\varphi'(R^-) = \varphi'(R^+) + \frac{\alpha Q^{\rm surf}}{R^2} {\rm e}^{(\lambda+\nu)/2}, \tag{48}$$

Eq. (46) and global neutrality condition $Q(\infty) = 0$, the metric element ν and electric field φ can be obtained by solving Eqs. (20), (33), and (36) along with the subsidiary conditions (21)–(25), (30) and (34).

3. Results and discussions

To fix the parameters of pQCD in Sec. 2.1, we adopt the latest results obtained by Particle Data Group [71], where the strong coupling constant at $M_Z = 91.1876$ GeV is given as $\alpha_s(M_Z) = 0.1185 \pm 0.0006$. Based on the continuity condition at the threshold of heavy quark masses and Eq. (6), we have $\Lambda_{\overline{\rm MS}} = 376.9^{+9.8}_{-9.6}$ MeV for $\bar{\Lambda} \leq m_c$. Meanwhile, at $\bar{\Lambda} = 2$ GeV, $m_u = 2.3^{+0.7}_{-0.5}$ MeV, $m_d = 4.8^{+0.5}_{-0.3}$ MeV, and $m_s = 95 \pm 5$ MeV [71]. If we take $\Lambda_{\overline{\rm MS}} = 376.9$ MeV, the invariant quark masses are obtained by solving Eq. (7), where $\hat{m}_u = 3.8^{+1.2}_{-0.8}$ MeV, $\hat{m}_d = 8.0^{+0.8}_{-0.5}$ MeV, and $\hat{m}_s = 158^{+9}_{-8}$ MeV. In this work, we take their central values, i.e., $\Lambda_{\overline{\rm MS}} = 376.9$ MeV, $\hat{m}_u = 3.8$ MeV, $\hat{m}_d = 8$ MeV, and $\hat{m}_s = 158$ MeV. The mass of electrons is taken as $m_e = 0.511$ MeV.

3.1. β-Stable SQM with charge neutrality

To see the properties of SQM with running masses and coupling constant, we first study the cases satisfying the β-stability condition in Eq. (18) and local charge neutrality condition

$$n_{\rm ch} = \sum_i q_i n_i = 0. \tag{49}$$

The particle number densities are obtained with Eq. (10), where the values of n_0 given by Eq. (13) are the same for all three types of quarks. Then Eq. (49) is converted into $\sum_{i=u,d,s} q_i n_i^* + q_e n_e = 0$ with n_i^* determined by Eq. (12). For given values of the total quark chemical potential $\mu \equiv \mu_u + \mu_d + \mu_s$, the chemical potentials are determined by fulfilling Eqs. (18) and (49). Then the properties of SQM are obtained with Eqs. (1)–(17).

In order for SQM objects to stably exist at zero external pressure, the Witten–Bodmer hypothesis [1,2] has to be fulfilled. The parameters C_0, C_1 and B are then constrained by requiring the minimum energy per baryon of quark matter smaller than 930 MeV for 3-flavor cases but larger for 2-flavor cases. The obtained results are presented in Fig. 1, where the parameters should lie

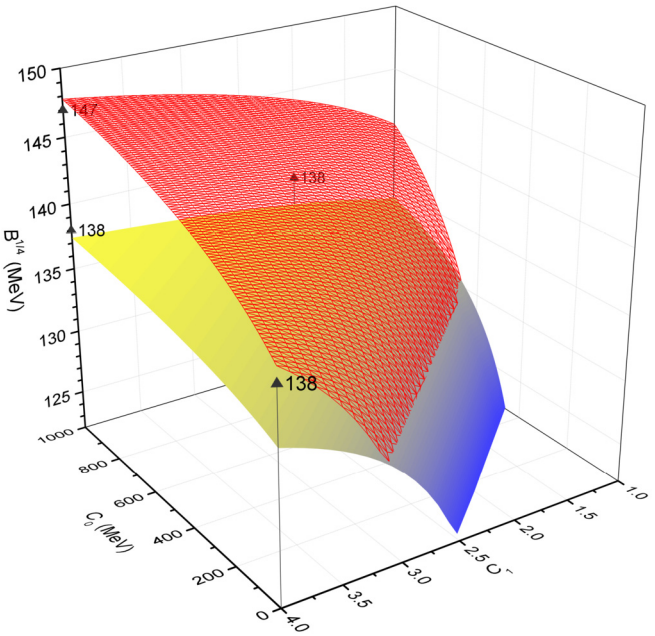

Fig. 1. (Color online.) Range of parameters C_0, C_1 and B that satisfies the Witten–Bodmer hypothesis, which lies in between the mesh and surface. The tetrahedra represent the selected parameter sets for our following studies.

in between the mesh and surface. For regions above the mesh and surface, SQM is unstable and can only exist at the center of compact stars, i.e., hybrid stars [15,72–77]. Note that the region beneath the surface is forbidden since 2-flavor quark matter can not be more stable than ^{56}Fe. As indicated by the tetrahedra, the parameter sets (C_0, C_1, $B^{1/4}$): (0, 4, 138), (1, 2, 138), (1, 4, 138), and (1, 4, 147) are chosen for our following study, where C_1 is dimensionless, C_0 in GeV and $B^{1/4}$ in MeV.

In Fig. 2, we present the baryon number density $n_\mathrm{b} = (n_u + n_d + n_s)/3$, strange quark mass m_s and strong coupling constant α_s as functions of μ. The choice of bag constant B is irrelevant here. As μ increases, n_b is increasing while m_s and α_s are decreasing. When we adopt larger values of C_0 and C_1, the baryon number density becomes larger. The running quark masses and strong coupling constant behave similarly with respect to μ. It is found that they decrease faster for smaller C_0 or larger C_1. Meanwhile, m_s and α_s are smaller if we take larger values of C_0 and C_1.

The energy per baryon E/n_b of SQM is presented in Fig. 3 as functions of baryon number density, where the energy density E is obtained with Eq. (17). Previously in [39, Eq. (10)], we have provided a necessary condition for thermodynamic self-consistency, i.e., $\triangle \equiv P - n_\mathrm{b}^2 \frac{\mathrm{d}}{\mathrm{d}n_\mathrm{b}} \left(\frac{E}{n_\mathrm{b}}\right) = 0$. In this work $\triangle$ remains zero for β-stable SQM with charge neutrality, suggesting that the thermodynamic self-consistency is satisfied. The properties of SQM at zero external pressure are presented in Table 1. Note that the total chemical potential μ coincides with the minimum energy per baryon. This is a nature consequence for SQM at zero pressure with the β-stability and charge neutrality conditions fulfilled. Since the parameters are chosen to meet the requirement of the Witten–Bodmer hypothesis, the obtained minimum energy per baryon of SQM is always smaller than 930 MeV. Meanwhile, the corresponding baryon number

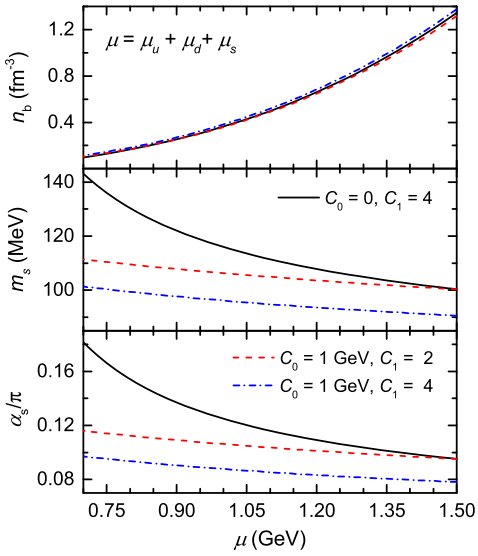

Fig. 2. (Color online.) Baryon number density (top), strange quark mass (middle) and strong coupling constant (bottom) as functions of the total quark chemical potential μ.

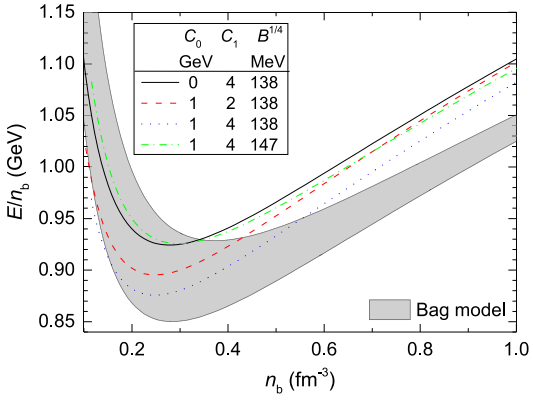

Fig. 3. (Color online.) Energy per baryon of SQM as functions of baryon number density. The shaded region corresponds to the results obtained with the bag model by varying the bag constant $B^{1/4}$ from 145 to 159 MeV, which lies within the stability window; the same convention is adopted for the following figures.

densities lie within the range $0.24 \lesssim n_b \lesssim 0.3$ fm^{-3}. At given values of C_0 and B, the SQM energy becomes smaller with larger C_1. Since the non-perturbative effects are important at lower densities, varying C_0 and B has more impact on SQM energy at lower densities than higher ones. If we increase C_0 or decrease B, the obtained energy per baryon is smaller. For comparison reason, in Fig. 3 we present the results obtained with the bag model. The energy per baryon obtained by incorporating the results from pQCD can be reproduced by bag model at lower densities, while this is not the case at higher densities since the perturbative interactions become important.

Table 1
Properties of SQM at zero external pressure.

C_0 GeV	C_1	$B^{1/4}$ MeV	n_b fm^{-3}	μ MeV	E/n_b MeV
0	4	138	0.278	924.23	924.23
1	2	138	0.248	895.39	895.39
1	4	138	0.247	875.64	875.64
1	4	147	0.297	925.63	925.63

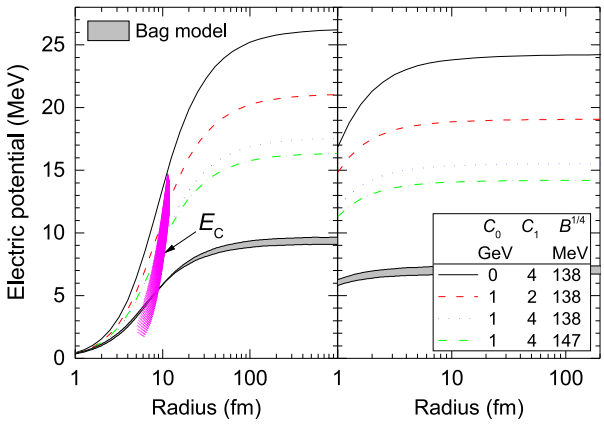

Fig. 4. (Color online.) Left: the electric potential $\varphi(R)$ on the quark-vacuum interface as functions of R, which is compared with the Coulomb barrier E_C for finite nuclei. Right: the electric potential φ_0 that fulfills the local charge neutrality condition $n_{ch}(\varphi_0, \nu_0) = 0$.

3.2. The properties of SQM objects

Based on the UDS model [56–58], we investigate the properties of SQM objects ranging from strangelets to strange stars. By adopting the simplifications in Secs. 2.2.1 and 2.2.2, the numerical calculation for SQM objects are greatly simplified. For example, the computational time to obtain the particle distribution of a strangelet with $R = 10$ fm are reduced by two orders of magnitude comparing to the straightforward calculation. The obtained mass, total particle numbers, and particle distributions are not affected by the simplifications. Note that we have adopted Eq. (36) for the electron cloud. At larger radii, the computational time can be further reduced if we consider massless electrons.

In the left panel of Fig. 4 we show the electric potential $\varphi(R)$ on the quark-vacuum interface, which is obtained with Eqs. (34) and (36) by fulfilling the global charge neutrality condition. The electric potential $\varphi(r)$ in the surface region can be obtained with Eq. (31), where the values of φ_0 and λ_D are presented in the right panel of Fig. 4 and in Fig. 5, respectively. Due to the effects of perturbative interactions, the electric potential and Debye screening length obtained with pQCD are much larger than those with bag model. At certain radii, as indicated in Fig. 4, the electric potential $\varphi(R)$ on the surface of SQM objects are even larger than the Coulomb barrier of finite nuclei for proton reactions $E_C = \alpha Z/R_e$ ($R_e = r_e A^{1/3} + R_p$ with $r_e = 1.62$ fm and $R_p = 1.443$ fm [78]). This may affect the search for SQM via heavy-ion activation [79, 80], where a low-energy beam of heavy ions can not penetrate the Coulomb barrier of an SQM

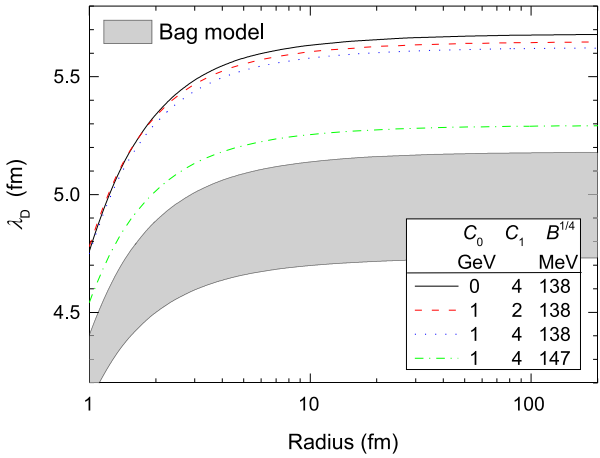

Fig. 5. (Color online.) The Debye screening length of SQM in the vicinity of the quark-vacuum interface.

Table 2
The properties of SQM objects at large radii and the maximum masses and radii of strange stars.

Parameters			$R \gtrsim 10^4$ fm					10^4 fm $\lesssim R \lesssim 1$ km		The most massive strange star				R_{max} km
C_0 GeV	C_1	$B^{1/4}$ MeV	$\mu(R)$ MeV	λ_D fm	$e\bar{\varphi}(R)$ MeV	$e\bar{\varphi}_0$ MeV	σ fm^{-2}	$\frac{M}{A}\Big\|_{sat}$ MeV	r_0 fm	$\frac{M}{A}\Big\|_{min}$ MeV	M_{max} $M_\odot$	A_{max} 10^{57}	R km	
0	4	138	924.22	5.68	26.29	24.23	0.100	924.23	0.95	774.76	1.79	2.58	10.04	10.50
1	2	138	895.37	5.65	21.10	19.07	0.065	895.39	0.99	750.36	1.93	2.88	10.82	11.32
1	4	138	875.63	5.62	17.59	15.54	0.045	875.64	0.99	732.85	1.98	3.01	11.03	11.52
1	4	147	925.62	5.29	16.39	14.21	0.040	925.63	0.93	774.20	1.77	2.54	9.81	10.25

object to produce the characteristic γ-rays. As the radius of an SQM core increases, the Debye screening length λ_D, the reduced electric potentials $\bar{\varphi}(R)$ and $\bar{\varphi}_0$ increase to the constant values indicated in Table 2. This suggests that the surface structures with the effects of gravity reduced are insensitive to radius for large enough SQM objects, i.e., $R \gtrsim 10^4$ fm.

To show more details on the surface structures of an SQM object, in Fig. 6 we present the total chemical potential of quarks $\mu(R) = \mu_u(R) + \mu_d(R) + \mu_s(R)$ on the quark-vacuum interface, which is determined by fulfilling the boundary condition in Eq. (46) as well as the β-stability condition in Eq. (18). The obtained results for pQCD coincide with bag model. Meanwhile, the values of $\mu(R)$ are decreasing with radius and approach to constants at $R \gtrsim 10^4$ fm as indicated in Table 2. If we take larger values of C_0 and C_1 or smaller B, $\mu(R)$ becomes smaller. According to Eq. (19), we have $\mu(r) = \bar{\mu}e^{-\nu(r)/2}$. The structure of an SQM object can then be obtained by solving Eq. (20) at given values of $\varphi(r)$. Note that $\mu(r)$ barely changes in the surface region with sizable $\varphi_S(r)$ ($R - 5\lambda_D \lesssim r < R$).

The mass-radius (M-R) relations of strange stars were investigated previously with perturbation models in Refs. [63–65]. The important effects of perturbative interactions on the structures of strange stars were pointed out, where the bag model is unlikely to predict a strange star with its mass exceeds $2M_\odot$ [65]. The statement coincides with our predictions here, where we have carefully fixed the parameters so that the Witten–Bodmer hypothesis is satisfied. As indicated in Fig. 7, the most massive strange stars predicted by bag model do not reach $2M_\odot$ unless we incorporate the results from pQCD. It is found that the masses and radii of strange stars are increasing

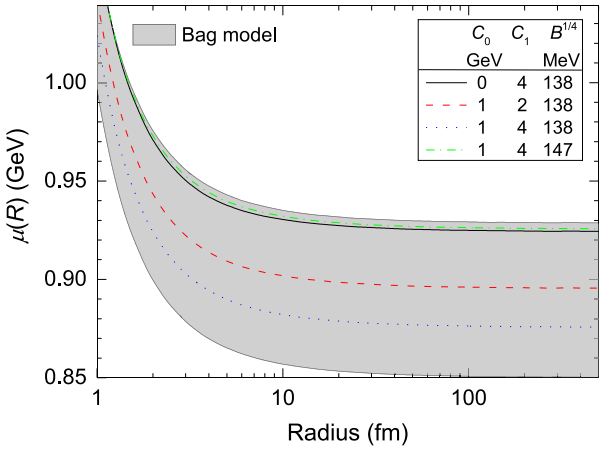

Fig. 6. (Color online.) The total quark chemical potential on the SQM core surface.

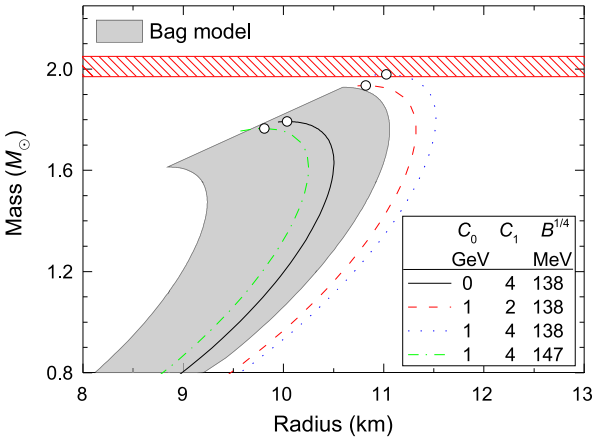

Fig. 7. (Color online.) The M-R relations of strange stars, where the most massive strange stars are marked with open circles. The mass of PSR J0348+0432 [62] is indicated with the horizontal band.

with C_0 and C_1 but decreasing with B. Note that the electric potential and surface structure have little effects on the mass and radius of a strange star so that the M-R relations in Fig. 7 do not deviate much from those predicted by conventional approaches.

The energy per baryon of an SQM object is presented in Fig. 8, which is decreasing with its baryon number. For strangelets, it is found that their masses obtained with and without perturbative interactions coincide with each other at certain choices of parameters. For moderate-sized SQM objects, their masses are insensitive to the effects of charge screening, quark depletion or gravity, where the energy per baryon in Fig. 8 varies little for $10^{12} \lesssim A \lesssim 10^{54}$. The corresponding values are indicated in Table 2 as $\frac{M}{A}\big|_{\rm sat}$, which coincide with these listed as $E/n_{\rm b}$ in Table 1. Meanwhile, the most massive strange stars in Fig. 7 correspond to these indicated with open circles in Fig. 8, suggesting that the most massive strange star has the minimum energy per baryon and the maximum baryon number. The minimum energy per baryon is found to be decreasing with C_0 and C_1 but increasing with B. Note that an SQM object is stable only if the energy per

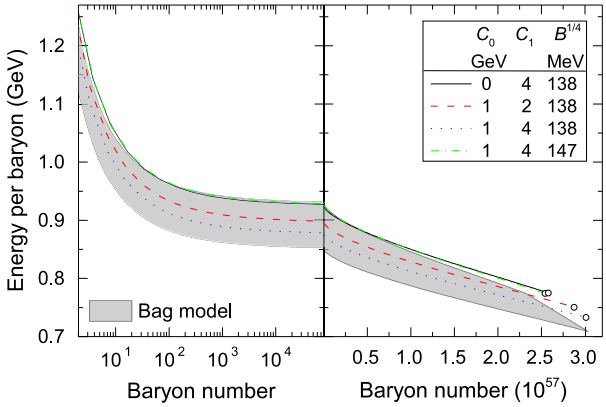

Fig. 8. (Color online.) The energy per baryon of SQM objects from strangelets to strange stars.

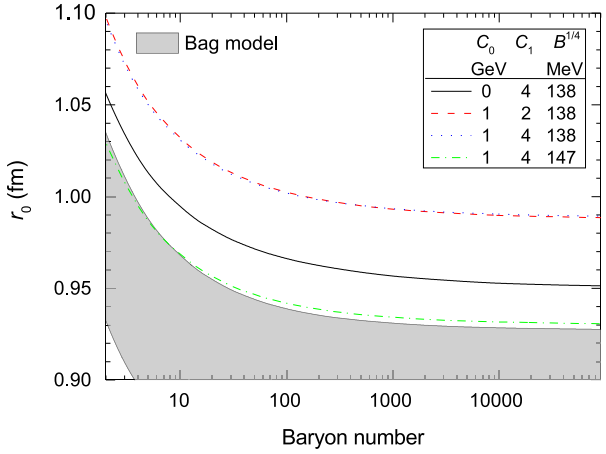

Fig. 9. (Color online.) The ratio of radius to baryon number $r_0 \equiv RA^{-1/3}$ for strangelets.

baryon is smaller than 930 MeV, suggesting the existence of a lower limit on the baryon numbers of stable SQM objects.

The dependence of the core radius R with respect to the baryon number A can be well described by the ratio of radius to baryon number r_0 with $R = r_0 A^{1/3}$. In Fig. 9 we present r_0 as functions of A for strangelets, where they become less compact when perturbative interactions are included. This will increase the energy loss when a nuclearite with $R \gtrsim 1$ Å passing through normal matter and consequently enhance the sensitivity for nuclearite detections [8,9,81,82]. For increasing baryon number, r_0 decreases to the constant values at $A \gtrsim 10^{12}$ as indicated in Table 2. Note that r_0 can be further reduced once gravity starts to take effect at $A \gtrsim 10^{54}$.

The most important observable for the search of SQM objects is the charge carried by them. In Fig. 10 we present the charge-to-mass ratio $f_Z = Q(R)/A$ and surface charge density $\sigma \equiv Q(R)/R^2$ for small SQM objects. It is found that the SQM objects become more positively charged once the perturbative interactions are included, which is mainly caused by the scale dependence of quark masses. The magnetic rigidity of a strangelet is decreased due to a larger f_Z, which may cause difficulties to distinguish strangelets from ordinary nuclei in mass spectrom-

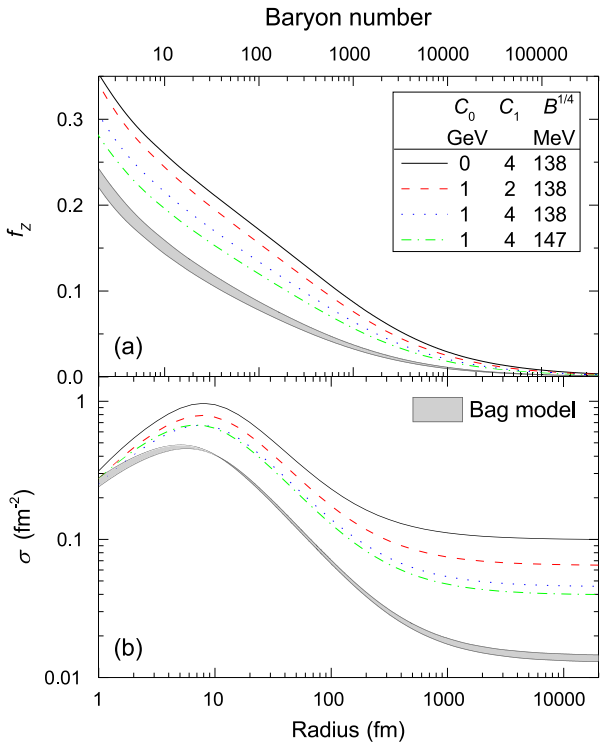

Fig. 10. (Color online.) The charge-to-mass ratio f_Z (a) and surface charge density σ (b) of small SQM objects.

eters [45,83–85]. The charge carried by an SQM object is reduced if we take larger values of C_0, C_1 and B. When the size of an SQM object is large enough ($R \gg \lambda_D$), charges are mostly located on the surface and are better described with a surface charge density σ, which is related to the charge-to-mass ratio by $f_Z = \sigma r_0^2 A^{-1/3}$ with r_0 given in Fig. 9. For increasing radius, as indicated in Fig. 10, σ first increases to its maximum value at $R \approx 8$ fm and starts to decrease at larger radius. The surface charge density approaches to a constant value at $R \gtrsim 10^4$ fm, which is indicated in Table 2.

4. Conclusion

We improved our recently proposed unified description for SQM objects, i.e., the UDS model. By adopting certain approximations, the numerical calculation was significantly simplified without loosing accuracy. The effects of perturbative interactions on the properties of SQM and SQM objects were investigated. It was found that the energy per baryon of β-stable SQM with charge neutrality can not be reproduced by bag model at higher densities, suggesting the important effects of perturbative interactions on stiffening the EoSs of SQM. For SQM objects, aside from the increase of masses and radii of strange stars, perturbative interactions also affect their charge properties. Particularly, the electric field became stronger and extended deeper into the core, while small SQM objects such as strangelets became less compact and more positively charged due to the effects of perturbative interactions. These will affect the sensitivity of the experimental searches for SQM. Finally, beside the perturbative interactions, it is worth mentioning that other

effects such as shell structures [6], non-spherical shapes [25], external magnetic field [86–89], and color superconductivity [90,91] may play important roles for the properties of SQM objects, which need to be considered in future works.

Acknowledgements

The authors thank Prof. Guang-Xiong Peng and Dr. Jian-Feng Xu for fruitful discussions. This work was supported by National Natural Science Foundation of China (Grant Nos. 11525524, 11621131001, and 11647601), National Key Basic Research Program of China (Grant No. 2013CB834400), and the Knowledge Innovation Project of the Chinese Academy of Sciences (Grant No. KJCX2-EW-N01). The computation of this work was supported by the HPC Cluster of SKLTP/ITP-CAS and the Supercomputing Center, CNIC of CAS.

References

[1] A.R. Bodmer, Phys. Rev. D 4 (1971) 1601–1606.
[2] E. Witten, Phys. Rev. D 30 (1984) 272–285.
[3] H. Terazawa, J. Phys. Soc. Jpn. 58 (1989) 3555–3563.
[4] E. Farhi, R.L. Jaffe, Phys. Rev. D 30 (1984) 2379–2390.
[5] M.S. Berger, R.L. Jaffe, Phys. Rev. C 35 (1987) 213–225.
[6] E.P. Gilson, R.L. Jaffe, Phys. Rev. Lett. 71 (1993) 332–335.
[7] G.X. Peng, X.J. Wen, Y.D. Chen, Phys. Lett. B 633 (2006) 314–318.
[8] A.D. Rújula, S.L. Glashow, Nature 312 (1984) 734.
[9] D.M. Lowder, Nucl. Phys. B, Proc. Suppl. 24 (1991) 177–183.
[10] J. Rafelski, L. Labun, J. Birrell, Phys. Rev. Lett. 110 (2013) 111102.
[11] N. Itoh, Prog. Theor. Phys. 44 (1970) 291–292.
[12] C. Alcock, E. Farhi, A. Olinto, Astrophys. J. 310 (1986) 261–272.
[13] P. Haensel, J.L. Zdunik, R. Schaeffer, Astron. Astrophys. 160 (1986) 121–128.
[14] R.-X. Xu, Astrophys. J. 596 (2003) L59.
[15] F. Weber, Prog. Part. Nucl. Phys. 54 (2005) 193–288.
[16] M.A. Perez-Garcia, J. Silk, J.R. Stone, Phys. Rev. Lett. 105 (2010) 141101.
[17] M. Herzog, F.K. Röpke, Phys. Rev. D 84 (2011) 083002.
[18] V. Dexheimer, J. Torres, D. Menezes, Eur. Phys. J. C 73 (2013) 2569.
[19] J.F. Xu, G.X. Peng, F. Liu, D.-F. Hou, L.-W. Chen, Phys. Rev. D 92 (2015) 025025.
[20] Y.-B. He, C.-S. Gao, X.-Q. Li, W.-Q. Chao, Phys. Rev. C 53 (1996) 1903–1910.
[21] Y.-B. He, W.-Q. Chao, C.-S. Gao, X.-Q. Li, Phys. Rev. C 54 (1996) 857–865.
[22] C. Greiner, P. Koch, H. Stöcker, Phys. Rev. Lett. 58 (1987) 1825–1828.
[23] C. Greiner, H. Stöcker, Phys. Rev. D 44 (1991) 3517–3529.
[24] J. Schaffner-Bielich, C. Greiner, A. Diener, H. Stöcker, Phys. Rev. C 55 (1997) 3038–3046.
[25] M.G. Mustafa, A. Ansari, Phys. Rev. C 56 (1997) 420–425.
[26] J. Madsen, Phys. Rev. Lett. 70 (1993) 391–393.
[27] J. Madsen, Phys. Rev. D 47 (1993) 5156–5160.
[28] J. Madsen, Phys. Rev. D 50 (1994) 3328–3331.
[29] M.G. Alford, K. Rajagopal, S. Reddy, A.W. Steiner, Phys. Rev. D 73 (2006) 114016.
[30] P. Jaikumar, S. Reddy, A.W. Steiner, Phys. Rev. Lett. 96 (2006) 041101.
[31] J. Madsen, Phys. Rev. Lett. 100 (2008) 151102.
[32] X.J. Wen, X.H. Zhong, G.X. Peng, P.N. Shen, P.Z. Ning, Phys. Rev. C 72 (2005) 015204.
[33] X.J. Wen, G.X. Peng, Y.D. Chen, J. Phys. G 34 (2007) 1697.
[34] S.-W. Chen, L. Gao, G.-X. Peng, Chin. Phys. C 36 (2012) 947.
[35] S.-W. Chen, G.-X. Peng, Commun. Theor. Phys. 57 (2012) 1037.
[36] Q. Chang, S.-W. Chen, G.-X. Peng, J.-F. Xu, Sci. China, Phys. Mech. Astron. 56 (2013) 1730.
[37] P.-C. Chu, L.-W. Chen, Astrophys. J. 780 (2014) 135.
[38] C.-J. Xia, S.-W. Chen, G.-X. Peng, Sci. China, Phys. Mech. Astron. 57 (2014) 1304.

[39] C.J. Xia, G.X. Peng, S.W. Chen, Z.Y. Lu, J.F. Xu, Phys. Rev. D 89 (2014) 105027.
[40] P.B. Price, E.K. Shirk, W.Z. Osborne, L.S. Pinsky, Phys. Rev. D 18 (1978) 1382–1421.
[41] C. Lattes, Y. Fujimoto, S. Hasegawa, Phys. Rep. 65 (1980) 151–229.
[42] T. Saito, Y. Hatano, Y. Fukada, H. Oda, Phys. Rev. Lett. 65 (1990) 2094–2097.
[43] M. Ichimura, E. Kamioka, M. Kitazawa, T. Kobayashi, T. Shibata, S. Somemiya, M. Kogawa, S. Kuramata, H. Matsutani, T. Murabayashi, H. Nanjyo, Z. Watanabe, H. Sugimoto, K. Nakazawa, Nuovo Cimento A 106 (1993) 843–852.
[44] R. Klingenberg, J. Phys. G 25 (1999) R273.
[45] E. Finch, J. Phys. G 32 (2006) S251.
[46] S. Burdin, M. Fairbairn, P. Mermod, D. Milstead, J. Pinfold, T. Sloan, W. Taylor, Phys. Rep. 582 (2015) 1–52.
[47] A. Hewish, S.J. Bell, J.D.H. Pilkington, P.F. Scott, R.A. Collins, Nature 217 (1968) 709–713.
[48] http://www.atnf.csiro.au/research/pulsar/psrcat/, ATNF Pulsar Catalogue.
[49] J.J. Drake, H.L. Marshall, S. Dreizler, P.E. Freeman, A. Fruscione, M. Juda, V. Kashyap, F. Nicastro, D.O. Pease, B.J. Wargelin, K. Werner, Astrophys. J. 572 (2002) 996.
[50] V. Burwitz, F. Haberl, R. Neuhäuser, P. Predehl, J. Trümper, V.E. Zavlin, Astron. Astrophys. 399 (2003) 1109–1114.
[51] Z.-S. Li, Z.-J. Qu, L. Chen, Y.-J. Guo, J.-L. Qu, R.-X. Xu, Astrophys. J. 798 (2015) 56.
[52] R. She, H. Feng, F. Muleri, P. Soffitta, R.-X. Xu, H. Li, R. Bellazzini, Z.-S. Wang, D. Spiga, M. Minuti, A. Brez, G. Spandre, M. Pinchera, C. Sgrò, L. Baldini, M.-W. Wen, Z.-X. Shen, G. Pareschi, G. Tagliaferri, K. Tayabaly, B. Salmaso, Y.-F. Zhan, Proc. SPIE 9601 (2015) 0I.
[53] R.D. Nan, D. Li, C.J. Jin, Q.M. Wang, L.C. Zhu, W.B. Zhu, H.Y. Zhang, Y.L. Yue, L. Qian, Int. J. Mod. Phys. D 20 (2011) 989–1024.
[54] K.C. Gendreau, Z. Arzoumanian, T. Okajima, Proc. SPIE 8443 (2012) 13.
[55] https://www.skatelescope.org/, The Square Kilometre Array.
[56] C.-J. Xia, G.-X. Peng, E.-G. Zhao, S.-G. Zhou, Sci. Bull. 61 (2016) 172–177.
[57] C.-J. Xia, Sci. Sin.-Phys. Mech. Astron. 46 (2016) 012021, in Chinese.
[58] C.-J. Xia, G.-X. Peng, E.-G. Zhao, S.-G. Zhou, Phys. Rev. D 93 (2016) 085025.
[59] A. Peshier, W. Cassing, Phys. Rev. Lett. 94 (2005) 172301.
[60] P.B. Demorest, T. Pennucci, S.M. Ransom, M.S.E. Roberts, J.W.T. Hessels, Nature 467 (2010) 1081–1083.
[61] E. Fonseca, T.T. Pennucci, J.A. Ellis, I.H. Stairs, D.J. Nice, S.M. Ransom, P.B. Demorest, Z. Arzoumanian, K. Crowter, T. Dolch, R.D. Ferdman, M.E. Gonzalez, G. Jones, M.L. Jones, M.T. Lam, L. Levin, M.A. McLaughlin, K. Stovall, J.K. Swiggum, W. Zhu, arXiv:1603.00545, 2016.
[62] J. Antoniadis, P.C.C. Freire, N. Wex, T.M. Tauris, R.S. Lynch, M.H. van Kerkwijk, M. Kramer, C. Bassa, V.S. Dhillon, T. Driebe, J.W.T. Hessels, V.M. Kaspi, V.I. Kondratiev, N. Langer, T.R. Marsh, M.A. McLaughlin, T.T. Pennucci, S.M. Ransom, I.H. Stairs, J. van Leeuwen, J.P.W. Verbiest, D.G. Whelan, Science 340 (2013) 6131.
[63] E.S. Fraga, P. Romatschke, Phys. Rev. D 71 (2005) 105014.
[64] A. Kurkela, P. Romatschke, A. Vuorinen, Phys. Rev. D 81 (2010) 105021.
[65] E.S. Fraga, A. Kurkela, A. Vuorinen, Astrophys. J. 781 (2014) L25.
[66] B.A. Freedman, L.D. McLerran, Phys. Rev. D 16 (1977) 1169–1185.
[67] J. Vermaseren, S. Larin, T. van Ritbergen, Phys. Lett. B 405 (1997) 327–333.
[68] G.X. Peng, Phys. Lett. B 634 (2006) 413–418.
[69] H. Heiselberg, Phys. Rev. D 48 (1993) 1418–1423.
[70] A. Migdal, D. Voskresenskii, V. Popov, JETP Lett. 24 (1976) 163–165.
[71] Particle Data Group, Chin. Phys. C 38 (2014) 090001.
[72] T. Maruyama, S. Chiba, H.-J. Schulze, T. Tatsumi, Phys. Rev. D 76 (2007) 123015.
[73] G.X. Peng, A. Li, U. Lombardo, Phys. Rev. C 77 (2008) 065807.
[74] G.-Y. Shao, M. Colonna, M. Di Toro, Y.-X. Liu, B. Liu, Phys. Rev. D 87 (2013) 096012.
[75] T. Klähn, R. Łastowiecki, D. Blaschke, Phys. Rev. D 88 (2013) 085001.
[76] T. Zhao, S.-S. Xu, Y. Yan, X.-L. Luo, X.-J. Liu, H.-S. Zong, Phys. Rev. D 92 (2015) 054012.
[77] A. Li, W. Zuo, G.X. Peng, Phys. Rev. C 91 (2015) 035803.
[78] L.C. Vaz, J.M. Alexander, Phys. Rev. C 10 (1974) 464–478.
[79] E. Farhi, R.L. Jaffe, Phys. Rev. D 32 (1985) 2452–2455.
[80] M.C.P. Isaac, Y.D. Chan, R. Clark, M.A. Deleplanque, M.R. Dragowsky, P. Fallon, I.D. Goldman, R.-M. Larimer, I.Y. Lee, A.O. Macchiavelli, R.W. MacLeod, K. Nishiizumi, E.B. Norman, L.S. Schroeder, F.S. Stephens, Phys. Rev. Lett. 81 (1998) 2416–2419.
[81] A.D. Rújula, Nucl. Phys. A 434 (1985) 605C.
[82] W.-L. Guo, C.-J. Xia, T. Lin, Z.-M. Wang, arXiv:1611.00166, 2016.

[83] Z.-T. Lu, R. Holt, P. Mueller, T. O'Connor, J. Schiffer, L.-B. Wang, Nucl. Phys. A 754 (2005) 361–368, Proceedings of the Eighth International Conference on Hypernuclear and Strange Particle Physics.
[84] K. Han, J. Ashenfelter, A. Chikanian, W. Emmet, L.E. Finch, A. Heinz, J. Madsen, R.D. Majka, B. Monreal, J. Sandweiss, Phys. Rev. Lett. 103 (2009) 092302.
[85] O. Adriani, G.C. Barbarino, G.A. Bazilevskaya, R. Bellotti, M. Boezio, E.A. Bogomolov, M. Bongi, V. Bonvicini, S. Bottai, A. Bruno, F. Cafagna, D. Campana, P. Carlson, M. Casolino, G. Castellini, C. De Donato, C. De Santis, N. De Simone, V. Di Felice, V. Formato, A.M. Galper, A.V. Karelin, S.V. Koldashov, S. Koldobskiy, S.Y. Krutkov, A.N. Kvashnin, A. Leonov, V. Malakhov, L. Marcelli, M. Martucci, A.G. Mayorov, W. Menn, M. Mergè, V.V. Mikhailov, E. Mocchiutti, A. Monaco, N. Mori, R. Munini, G. Osteria, F. Palma, B. Panico, P. Papini, M. Pearce, P. Picozza, M. Ricci, S.B. Ricciarini, R. Sarkar, V. Scotti, M. Simon, R. Sparvoli, P. Spillantini, Y.I. Stozhkov, A. Vacchi, E. Vannuccini, G. Vasilyev, S.A. Voronov, Y.T. Yurkin, G. Zampa, N. Zampa, Phys. Rev. Lett. 115 (2015) 111101.
[86] R.G. Felipe, E.L. Fune, D.M. Paret, A.P. Martinez, J. Phys. G 39 (2012) 045006.
[87] X.-J. Wen, S.-Z. Su, D.-H. Yang, G.-X. Peng, Phys. Rev. D 86 (2012) 034006.
[88] J.-X. Hou, G.-X. Peng, C.-J. Xia, J.-F. Xu, Chin. Phys. C 39 (2015) 015101.
[89] A.A. Isayev, Phys. Rev. C 91 (2015) 015208.
[90] J. Madsen, Phys. Rev. Lett. 87 (2001) 172003.
[91] M. Oertel, M. Urban, Phys. Rev. D 77 (2008) 074015.